Timing the start of division in *E. coli*: a single-cell study

2008 Phys. Biol. 5 046001

(http://iopscience.iop.org/1478-3975/5/4/046001)

Phys. Biol. **5** (2008) 046001 (9pp) doi:10.1088/1478-3975/5/4/046001

Timing the start of division in *E. coli*: a single-cell study

G Reshes[1,2], S Vanounou[2], I Fishov[3] and M Feingold[1,2]

[1] Department of Physics, Ben Gurion University, Beer Sheva 84105, Israel
[2] The Ilse Katz Center for Nanotechnology, Ben Gurion University, Beer Sheva 84105, Israel
[3] Department of Life Sciences, Ben Gurion University, Beer Sheva 84105, Israel

E-mail: mario@bgu.ac.il

Received 11 June 2008
Accepted for publication 25 September 2008
Published 7 November 2008
Online at stacks.iop.org/PhysBio/5/046001

Abstract

We monitor the shape dynamics of individual *E. coli* cells using time-lapse microscopy together with accurate image analysis. This allows measuring the dynamics of single-cell parameters throughout the cell cycle. In previous work, we have used this approach to characterize the main features of single-cell morphogenesis between successive divisions. Here, we focus on the behavior of the parameters that are related to cell division and study their variation over a population of 30 cells. In particular, we show that the single-cell data for the constriction width dynamics collapse onto a unique curve following appropriate rescaling of the corresponding variables. This suggests the presence of an underlying time scale that determines the rate at which the cell cycle advances in each individual cell. For the case of cell length dynamics a similar rescaling of variables emphasizes the presence of a breakpoint in the growth rate at the time when division starts, τ_c. We also find that the τ_c of individual cells is correlated with their generation time, τ_g, and inversely correlated with the corresponding length at birth, L_0. Moreover, the extent of the T-period, $\tau_g - \tau_c$, is apparently independent of τ_g. The relations between τ_c, τ_g and L_0 indicate possible compensation mechanisms that maintain cell length variability at about 10%. Similar behavior was observed for both fast-growing cells in a rich medium (LB) and for slower growth in a minimal medium (M9-glucose). To reveal the molecular mechanisms that lead to the observed organization of the cell cycle, we should further extend our approach to monitor the formation of the divisome.

M This article features online multimedia enhancements

1. Introduction

Division is the concluding event of the cell cycle leading to the formation of two separate entities that each receives a copy of the parental genetic material. In bacteria, it typically overlaps with growth and chromosome replication [8]. Its starting point may be associated either with the formation of the FtsZ ring or, alternatively, with the initiation of envelope constriction, τ_c [2]. Proper determination of these times is necessary for understanding the checkpoints in cell cycle regulation. In particular, it is unclear whether an additional signal is required to activate the divisome after its assembly on the FtsZ ring or whether envelope constriction starts immediately after maturation [1]. In this work, we present a detailed morphological characterization of the cell division process and ways in which it varies from one cell to another. We show that the parameters that describe cell division obey certain quantitative relations. This information provides new constraints on the possible molecular mechanisms involved in the formation of both the divisome and the cell septum.

τ_c has been traditionally measured by visual inspection of cell images obtained from light or electron microscopy [2]. While in the case of light microscopy this approach suffers from the limitation due to optical resolution, electron microscopy cannot provide timing information. This suggests that, in most studies performed using light microscopy, τ_c

has been overestimated. For *E. coli*, we have recently developed a new approach that circumvents the resolution limit establishing the position of the cell edge with sub-pixel precision [13]. Our approach relies on calibrating the phase contrast intensity value in the pixels located at the cell boundary. This method can be used to achieve a significantly improved estimate for the value of τ_c. We find that it occurs much earlier than the appearance of a visible constriction [13]. This method was also used to measure growth dynamics at the single-cell level [14, 9]. Following cell elongation with high temporal resolution together with the reliable τ_c leads us to identify a break in the length dynamics corresponding to the initiation of new pole formation. Here, we further expand our analysis to show that this behavior is generic for all bacteria in a steady state population. We also present evidence that some of the cell cycle parameters are related to each other.

In [13], we described in detail the technical aspects of the image analysis methods that allow us to obtain cell contours with sub-pixel accuracy and determine τ_c. Moreover, we used this approach to analyze the entire life cycle of single *E. coli* cells in LB. We found that about half the cells grow in two regimes separated by τ_c, while the other half displays an additional break point in the growth curve at $\tau_2 > \tau_c$. Here, we describe the results of new experiments and focus on the part of the cell cycle around τ_c. In particular, we present the results of experiments performed at a slower average growth rate (in M9-glucose) and show that the measured behavior is analogous to that found for fast-growing cells. In the analysis of the data we also introduce several new observations. First, we use simple rescaling of variables to provide a global view of the entire cell population. This allows us to visually compare the variation of specific cell cycle features over the population. In particular, we show that the data for the dynamics of the constriction width for all the cells in the population collapse to the vicinity of the function predicted by our theoretical model. Second, we found that τ_c is correlated with both τ_g, the generation time, and L_0, the cell length at birth. To a good approximation, it grows linearly with τ_g and decreases linearly with L_0. These relations indicate that compensation mechanisms control the start of division to prevent excessive variability between cells. Third, we show that the extent of the T-period, $\tau_g - \tau_c$, is roughly constant. Finally, we performed new experiments similar to those described in [13] using a slightly improved protocol. Although we use the same *E. coli* strain as in [13] (see methods) that includes a plasmid with HU-GFP for imaging the nucleoid, in the new experiments, unlike in [13], no inducer (arabinose) is used. While the overall behavior is the same as before, we find that the variability of the cell cycle parameters is reduced in the absence of the inducer. This is probably due to the lower load on the cell resources when there is no expression from the HU-GFP plasmid.

The precision of our contour-finding algorithm was also improved over that of [13] (see [10] for a detailed description of the upgraded contour finding method). Presently, the error in locating a contour point is only 31 nm. In what follows, we will avoid, whenever possible, discussing behavior associated with the second break point in $L(t)$ that occurs at τ_2. Since the two break points, τ_c and τ_2, are determined by different peptidoglycan growth networks, this choice was made for the sake of simplicity and clarity of exposition. Nevertheless, one may refer to [13] for the basic phenomenology related to τ_2.

2. Materials and methods

2.1. Bacterial strains and growth conditions

Strain MW162 of *E. coli* K-12 [18] was grown either in LB medium or in M9 minimal salt medium supplemented with 0.4% glucose, both with ampicilin (100 μg ml^{-1}). Bacteria were cultivated at 37 °C with vigorous shaking up to $OD_{600} = 0.2$ in the exponential growth regime. In calibration experiments, the cytoplasmic membrane (CM) was stained with 1 μM FM4-64 (Molecular Probes) after fixation with 0.2% formaldehyde.

For microscopy, we apply 10 μl of exponential bacterial culture on a thin layer of 1.5% agar with LB (Sigma) or prepared on the M9-glucose medium. Measurements start only after one division is completed and we avoid analyzing cells that are too far along the division process at the start of the experiment. As a result, data are collected no less that 10 min after the cells are shifted to agar for fast-growing conditions (LB) and no less than 20 min for slow-growing cells (M9-glucose). Growth of individual bacteria (a total of 30) was monitored during at least two cell cycles. We have verified that cells grow at a steady state on the agar. This was done by monitoring about nine generations of a micro-colony originating from a single-cell, and counting the number of cells, N, as a function of time (data not shown). We find that up to five generations, the growth of N is exponential. In LB, the average doubling time for the 30 cells was 18.10 $\pm$ 0.52 min which is consistent with the generation time measured by monitoring OD_{600} of the corresponding liquid culture, 22.27 $\pm$ 0.69 min. The corresponding times for cells grown in M9-glucose were 38.38 $\pm$ 1.10 min and 48.64 $\pm$ 1.61 min, respectively. Although the difference between the generation times is significant (about 20% for both LB and M9-glucose), the faster growth rate on agar indicates that the solid support does not restrict cell growth.

2.2. Microscopy

Imaging experiments are performed on an inverted Olympus microscope (IX70) with a Micromax 512 camera (Princeton Instruments) and two computer controlled shutters (Uniblitz). One shutter blocks the mercury lamp and the other the halogen lamp. The appropriate shutter opens only for the duration of the exposure time. Time-lapse movies were recorded at 12 frames min^{-1}. Exposure time was fixed to 0.5 s. In our optical system, the pixel size corresponds to a length of 87 nm. The sample is heated by a resistor wrapped around the objective (Minco). A feedback system stabilizes the temperature within $\sim$0.5 °C. All experiments were performed at 37 °C. The drift of the focus is manually corrected throughout the experiment.

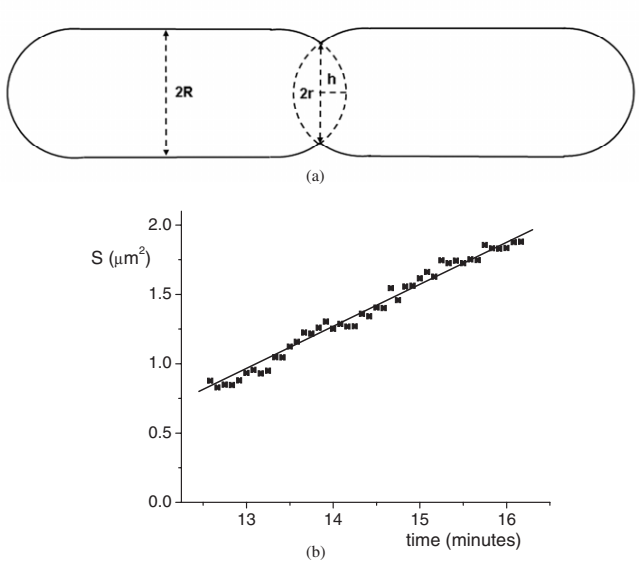

Figure 1. (*a*) Geometrical model of the *E. coli* cell that leads to equation (1). (*b*) The dynamics of the septal area, $S(t)$, for a typical cell (squares). The best linear fit to the data is also shown (line).

2.3. Finding the edge of the bacterium

In order to establish the cell dimensions, it is necessary to find the position of the cell edge from phase contrast images. We have developed a method for high precision cell edge detection (HPCED) that was described in detail in [10, 13]. Briefly, it relies on the threshold value, I_{th}, for the phase contrast intensity that corresponds to the cell edge. This threshold is obtained by comparing the phase contrast image with the corresponding fluorescence image of the CM for the same cell. I_{th} represents the average value of the phase contrast intensity along the contour where fluorescence is maximal. We use interpolation of the pixel intensity values both in phase contrast and fluorescence in order to reach sub-pixel precision. The average position error of a point on the cell edge contour that is obtained using HPCED is as small as 31 nm (36% of a pixel). The cell contour is computed using a MATLAB program. This program also automatically detects and measures the width of the constriction defined as the smallest distance between two contour points that belong to the opposite sides of the cell cylindrical sector. The cell length is defined as the largest distance between two contour points.

3. Results

3.1. Septum dynamics

We use our high-precision cell edge detection (HPCED) method to monitor the dynamics of constriction in single live cells growing in LB [13]. On the other hand, in order to obtain a quantitative description of this process, we exploit the current view of the *E. coli* cell shape and division [12, 17] to develop a simple model. It involves the following four assumptions (figure 1(*a*)): (1) the cell is shaped as a cylinder with hemispherical caps; (2) at intermediate times during division, the constriction consists of two symmetric incomplete hemispheres; (3) the cell width, R, is constant throughout the cell cycle; (4) the area of the constriction, S, grows at a constant rate. Figure 1(*b*) illustrates the typical measured variation of $S(t)$ which is in good agreement with the last of our four assumptions. Moreover, from the last two assumptions one can show that the height of the missing part of the new cap, $h(t)$, decreases linearly in time. Notably, this means that the cell length increase due to the constriction is linear in time. From the geometry of figure 1(*a*) we obtain that the relative waist width, W, follows

$$W \equiv \frac{r}{R} = \sqrt{1 - \left(\frac{t - \tau_c}{\tau_g - \tau_c}\right)^2}, \qquad (1)$$

where $2r$ is the measured waist width, τ_c is the time when constriction starts and τ_g is the time between successive divisions. In previous work, we showed that the measured values of W for individual cells are in good agreement with the corresponding best fit of equation (1) (see figure 8 of [13]). The fit also provides the values of both τ_c and τ_g. We found that τ_c is significantly smaller than the time when constriction becomes visible, τ_{cv}. The latter is the earliest time when the presence of the constriction can be identified by visual inspection of the phase contrast image. τ_{cv} also represents the time when we start measuring W and corresponds to values of W between 0.9 and 0.95 (see figure 2(*a*)). Moreover, the value of τ_g obtained from the fit agrees within experimental error with that obtained from direct observation of successive divisions for the same cell. For the cell of figure 1(*b*), $\tau_c = 9.94 \pm 0.47$ min, $\tau_{cv} = 12.59 \pm 0.17$ min and $\tau_g = 17.25 \pm 0.27$ min.

The behavior of $S(t)$ (figure 1(*b*)) and $W(t)$ (figure 8 of [13]) is typical of the 30 cells that were analyzed. It is not clear, however, whether one can expect this to translate into a quantitative attribute. The main difficulty in comparing the data from different cells stems from the intrinsic variability in the values of τ_c and τ_g in a steady state population. This is illustrated in figure 2(*a*) where the $W(t)$ data for all our 30 cells are shown. To obtain a more transparent representation of this information, we may follow the traditional approach of bacterial physiology and average the single-cell data. However, in the context of a bacterial population, averaging is a troublesome approach smearing the variability and therefore hiding the mechanisms that lead to its emergence. Indeed, as may be expected from figure 2(*a*), straightforward averaging of the measured $W(t)$ leads to an oscillatory behavior that is clearly due to the limited size of the population (see Supporting Data, figure S1, available in the online version of the journal at stacks.iop.org/PhysBio/5/046001). Moreover, for times larger than the smallest τ_g, $\tau_{g,\min}$, cells that have divided drop out of the average. That is, for $t > \tau_{g,\min}$, the average is taken over a progressively smaller number of cells. To avoid the latter problem, we may normalize the time to the generation time, τ_g, before averaging. Using this approach we obtain the behavior shown in figure 2(*b*). The data of figure 2(*b*) represent an approximation to the average of $W(t/\tau_g)$, $\bar{W}(t/\tau_g)$. Although the latter is a well-defined function for a steady state population, it does not provide direct information about the septal dynamics in each individual cell. In particular, it significantly differs from the

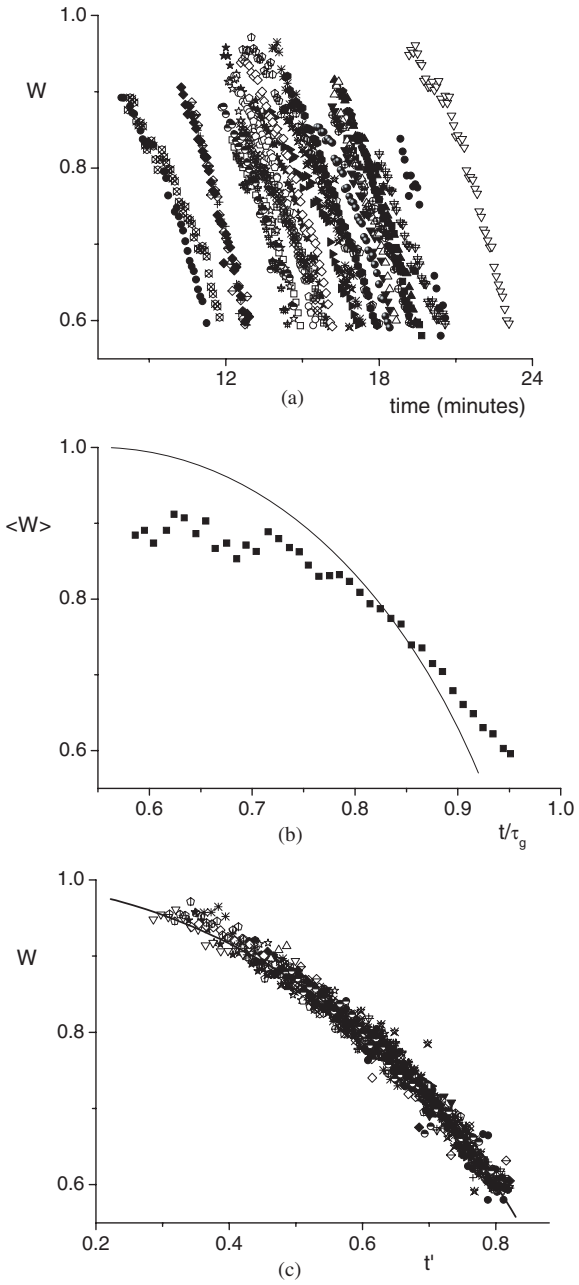

Figure 2. Behavior of the relative width of the constriction, W, as a function of time. (a) The measured $W(t)$ for the entire population of 30 cells (different symbols are used for different cells). (b) The average of $W(t/\tau_g)$, $\langle W(t/\tau_g)\rangle$ (squares) is compared to the prediction of equation (1) where the ratio τ_c/τ_g is replaced with the ratio of the corresponding average values, $\langle\tau_c\rangle/\langle\tau_g\rangle$ (see table 1) (solid line). (c) The same data as in (a) only now plotted as a function of the rescaled time, t', are compared to the prediction of equation (1) (solid line). The range of measured W is restricted due to the limitations of our method. For W close to unity, measurement starts when the program resolves the presence of the constriction. This happens at about the time when the constriction becomes visible. At the other end, our calibration of the phase contrast intensity was found to fail when the depth of the constriction approaches half the cell radius. In (a) and (c), a total of 1073 data points are displayed.

prediction of equation (1) with τ_c and τ_g replaced by their average values, $\langle\tau_c\rangle$ and $\langle\tau_g\rangle$, respectively (see figure 2(b)). To derive $\bar{W}(t/\tau_g)$, one needs to average equation (1) using the appropriate distributions of τ_c and τ_g. Alternatively, dynamics data from different cells can be rescaled to obtain a unified functional structure that incorporates the variabilities of both τ_c and τ_g [16]. For $W(t)$, this is achieved via a simple rescaling of the time variable. It leads to the collapse of the data for W from the entire cell population to the vicinity of a single curve.

As suggested by equation (1), we define a rescaled time, $t' = (t-\tau_c)/(\tau_g-\tau_c)$ for $\tau_c \leqslant t \leqslant \tau_g$, and plot the relative waist width as a function of t' (figure 2(c)). t' represents the fractional time of the division process. Figure 2(c) illustrates that all the cells that we analyzed follow the prediction of equation (1).

3.2. Cell length dynamics

In this section, we consider the elongation dynamics of individual cells growing in LB. It was shown that a change in the single-cell rate of growth occurs at times that, within experimental error, coincide with the corresponding values of τ_c as obtained from the septum dynamics [13]. This manifests as a breakpoint in $L(t)$. Assuming that the cylindrical part grows at a constant rate throughout the cell cycle and that growth of the new poles starts at τ_c, the latter will add to the overall elongation process, resulting in a distinctive change in the rate of cell growth at this time. Conversely, the breakpoint in the elongation dynamics may be used to confirm the τ_c values that are predicted using equation (1). The growth rate at $t > \tau_c$, a_2, is due both to that of the cylinder, a_1, and that of the new poles, a_h, and therefore we expect that $a_2 = a_1 + 2a_h$. This relation holds to a good approximation for all measured cells in the population [13]. Moreover, it roughly holds on average, $\langle a_2\rangle = 0.183 \pm 0.005$ μm min^{-1} and $\langle a_1 + 2a_h\rangle = 0.211 \pm 0.006$ μm min^{-1}. The difference between the two values may be due to a weak slowdown (13%) in the rate of cylindrical growth after τ_c. This is consistent with the recent evidence that penicillin-binding protein 2 (PBP2) which is part of the cylindrical growth machinery also participates in the initial stages of septum formation [3]. This may lead to a certain degree of competition between cylindrical and septal growth.

In figure 3(a), we illustrate the growth dynamics of the entire analyzed population. As in section 3.1, it is difficult to extract the useful information from this representation. Moreover, direct averaging over the population is problematic since for $t > \tau_{g,\min}$ cells start to drop out of the average (see Supporting Data, figure S2, available in the online version of the journal at stacks.iop.org/PhysBio/5/046001). Therefore, we use the same approach as in the previous section and average using the normalized time, t/τ_g (see figure 3(b)). As one may expect, the averaging smears out the break point leading to a smooth curve for $\langle L(t/\tau_g)\rangle$. To preserve the single-cell features and also display the $L(t)$ for the whole population, we may use rescaled variables. Since to a good approximation $L(t)$ grows linearly at a rate a_1 until τ_c, we define a new length as $L' = (L - L_0)/a_1\tau_c$ and new time, $t' = t/\tau_c$, where L_0 is the cell length at birth. Such rescaling emphasizes the existence of a joint break point in $L(t)$ for all cells despite the

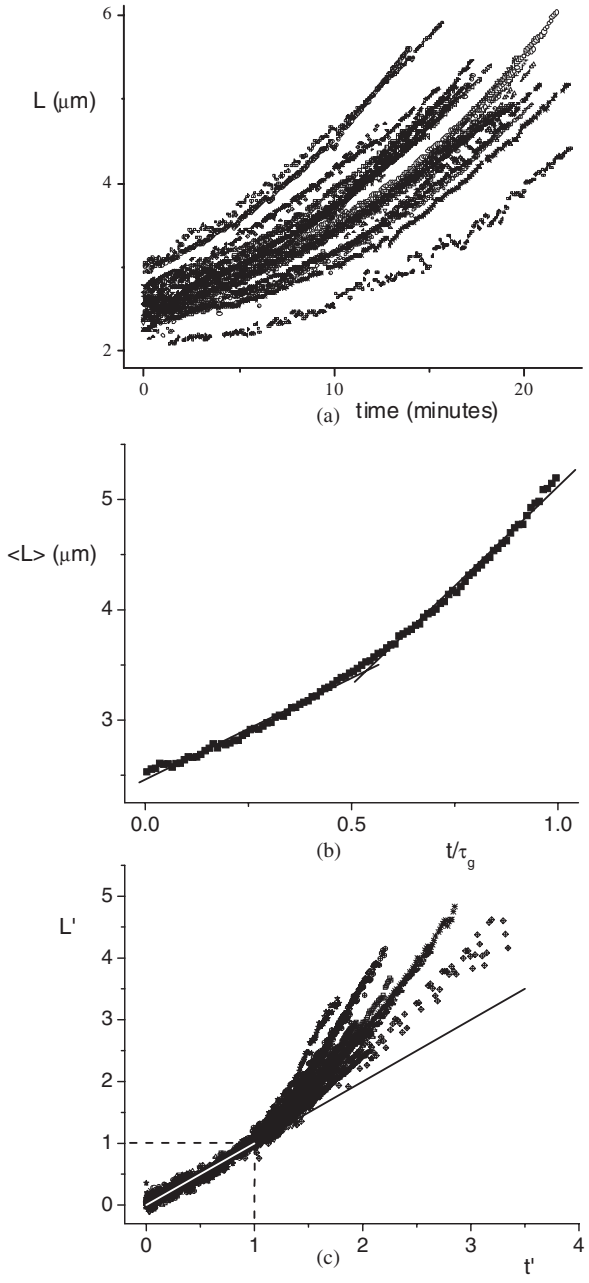

Figure 3. Behavior of the cell length, $L(t)$. (a) The measured $L(t)$ for 28 cells. The total number of data points displayed in this figure is 5526. Two cells that had unusually large values of τ_c are not included. (b) The average of $L(t/\tau_g)$, $\langle L(t/\tau_g)\rangle$ is shown together with the corresponding best fitting lines for $\frac{t}{\tau_g} < \frac{\langle\tau_c\rangle}{\langle\tau_g\rangle}$ and $\frac{t}{\tau_g} > \frac{\langle\tau_c\rangle}{\langle\tau_g\rangle}$ (solid lines). (c) The same data as in (a) are plotted here in terms of the rescaled variables, L' and t', as described in the text.

variabilities of τ_c and a_1 (see figure 3(c)). This break point is located in the neighborhood of $(t', L') = (1, 1)$ indicating that τ_c is the time when a discontinuous change in the cell growth rate takes place. While the data in the (0, 1) interval are collapsed together, for $t' > 1$ it fans out to a range of slopes that are all larger than unity. The latter is a direct consequence of a_2 variability and the fact that $a_2 > a_1$. If we were to use another time for rescaling instead of τ_c, for example the time of visible constriction, τ_{cv}, the break point would be significantly displaced from (1, 1) (not shown).

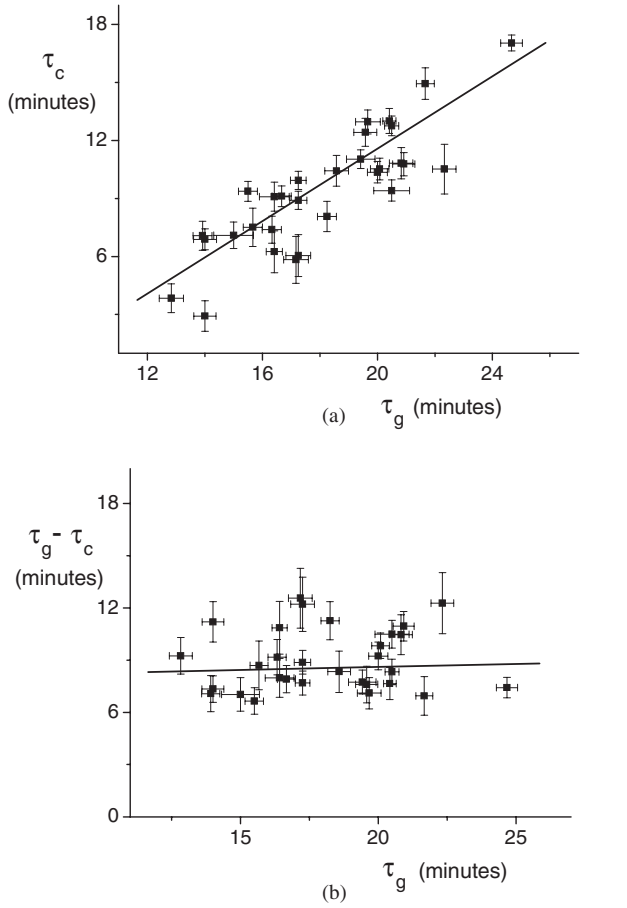

Figure 4. Relations between (a) τ_c and τ_g (b) $\tau_g - \tau_c$ and τ_g for the entire 30 cell population (squares). The corresponding linear fits are also shown (solid line).

3.3. Variability of the single-cell constriction time, τ_c

Our measurements allow one to obtain the characteristic parameters of individual bacteria. In particular, we measure the times of initiation and completion of division. Even though we analyzed a relatively small population, we found that these times significantly vary from cell to cell, CV $(\tau_c) = 0.33$ and CV $(\tau_g) = 0.16$. We note however, that the values of τ_c and τ_g are correlated (figure 4(a)). This fact may be interpreted as due to an underlying time scale that determines the rate at which a particular cell develops. In other words, the overall doubling time of a cell is to a large extent determined by the time of division initiation. The complementary aspect of this statement is the approximate independence of the duration of division, $\tau_g - \tau_c$, known as the T-period, on the doubling time (figure 4(b)). The latter stems from the relatively low variability of R (CV $= 0.04$), the independence of a_h on τ_g (not shown) and from the fact that $a_h = R/(\tau_g - \tau_c)$ (see figure 16 in [13]). In this respect, our single-cell measurements are in agreement with results obtained from bacterial populations (reviewed in [8]).

The relation between τ_c and τ_g may also be viewed as a form of compensation whereby the slower cells allow for larger division times. However, compensation manifests more directly in the correlation we find between τ_c and $L_0 \equiv L(0)$,

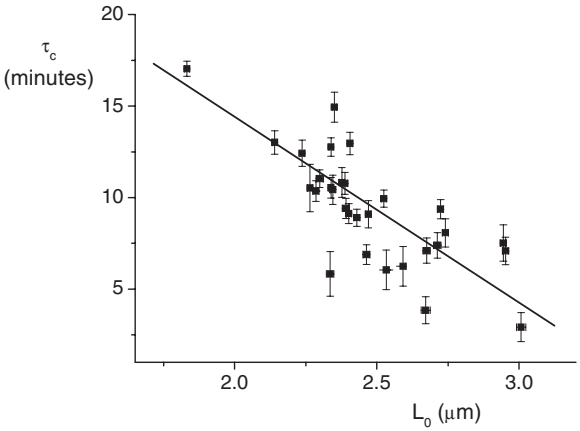

Figure 5. Relation between τ_c and L_0 for the entire population (squares). The corresponding linear fit is also shown (solid line). Note that the error of L_0 is barely larger than the size of the symbol.

Table 1. Growth parameters for bacteria grown in LB that display bimodal growth. D is the cell diameter, times are in minutes, growth rates are in μm min^{-1} and lengths are in μm.

Parameter	Mean	SD	CV
τ_c	9.721	3.187	32.788
τ_g	17.622	3.111	17.654
$\tau_g - \tau_c$	8.017	1.043	13.006
a_1	0.111	0.018	15.947
a_2	0.190	0.029	15.148
a_h	0.057	0.007	11.768
L_0	2.482	0.274	11.028
$L(\tau_c)$	3.547	0.316	8.914
$L(\tau_g)$	5.034	0.402	7.99
D	0.933	0.043	4.586

the cell length at birth. In particular, cells that are relatively short at birth appear to initiate division later in their life cycle (see figure 5). As L_0 grows, division occurs gradually earlier (smaller τ_c) leading to a roughly linear dependence for $\tau_c(L_0)$. This behavior suggests that cells tend to reach a certain length range before they divide. Such a control mechanism would allow cell populations to maintain cell size variability within bounds.

3.4. Behavior at a slower growth rate

We have further applied our analysis to a similar cell population that is grown in minimal medium (M9-glucose) corresponding to an average generation time, τ_g, that is about twice that in the rich medium (LB, see tables 1 and 2). We find that the slow-growing cells behave to a large extent analogously to those of the fast-growing population (see figures 6–8). In figure 6, the collapsed data for $W(t')$ of individual cells that were grown in M9-glucose are shown to also cluster around the prediction of equation (1). Moreover, figure 7 describes an approximately linear dependence of τ_c on τ_g and an apparent independence of the extent of the T-period on τ_g. Figures 6 and 7 represent the slow growth analogs of figures 2(c) and 4, respectively. On the other hand,

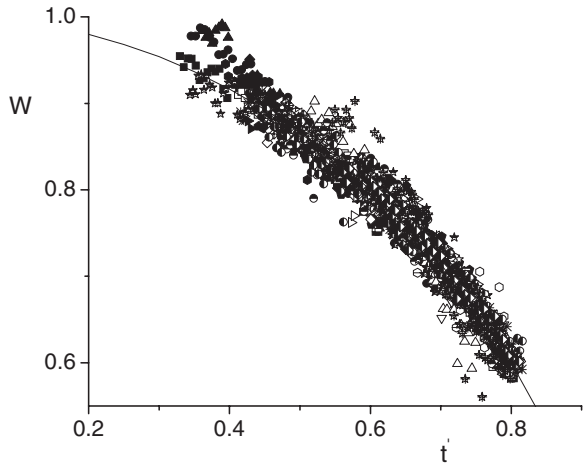

Figure 6. Same as in figure 2(c) except that here cells grow in minimal medium (M9-glucose).

Table 2. Same as in table 1 except that here cells grow in M9-glucose.

Parameter	Mean	SD	CV
τ_c	18.726	5.564	29.713
τ_g	36.816	4.761	12.931
$\tau_g - \tau_c$	18.934	3.455	18.249
a_1	0.029	0.007	24.071
a_2	0.055	0.009	15.423
a_h	0.019	0.004	21.334
L_0	1.607	0.178	11.103
$L(\tau_c)$	2.135	0.218	10.192
$L(\tau_g)$	3.126	0.247	7.887
D	0.716	0.047	6.518

the compensation between τ_c and L_0 that was found in fast-growing cells (LB, figure 5) is almost absent for those grown in M9-glucose (see figure 8).

In tables 1 and 2, we compare the average parameters and the corresponding standard deviations for cells grown in the rich medium (LB) and in the minimal medium (M9-glucose), respectively. Note that the two-fold difference in generation and constriction times is accompanied by a larger change in the elongation rates, apparently in accordance with the size differences. In addition, the variabilities of the primary elongation rate, a_1, and the septation rate, a_h, are higher at the low growth rate, probably due to larger fluctuations in the relative distribution of constituents in smaller cells.

4. Discussion

Using HPCED, we monitor the dynamics of cell shape with high spatial and temporal accuracy. This allows determining the true time for the initiation and completion of division. In [13], we have discussed the experimental errors for τ_c and τ_g; the average error for τ_c is 0.72 min and for τ_g it is 0.38 min.

It is worthwhile to note that the constriction closure as predicted by equation (1) and verified by our measurements and their collapse ((figures 2(c), 6 and 8 of [13]) proceeds at a different rate close to initiation than toward completion. In

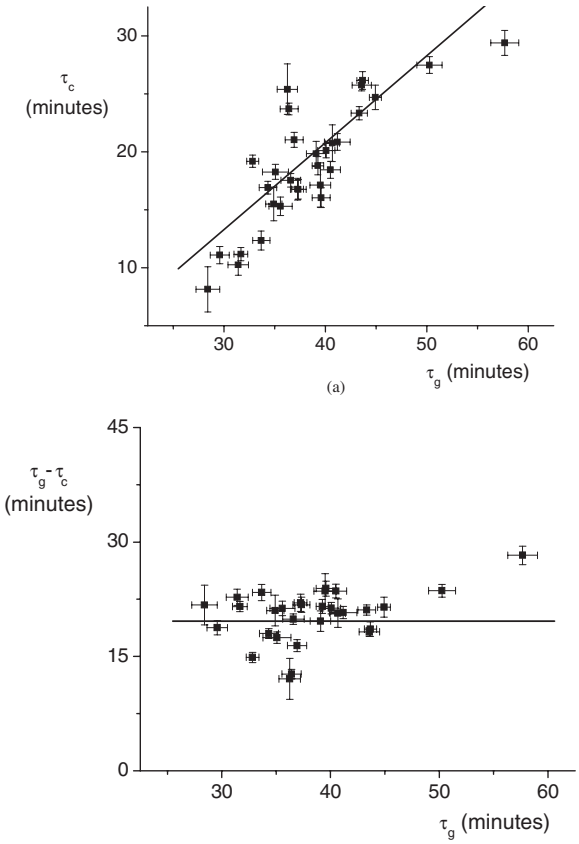

Figure 7. Same as in figure 4 except that here cells grow in minimal medium (M9-glucose).

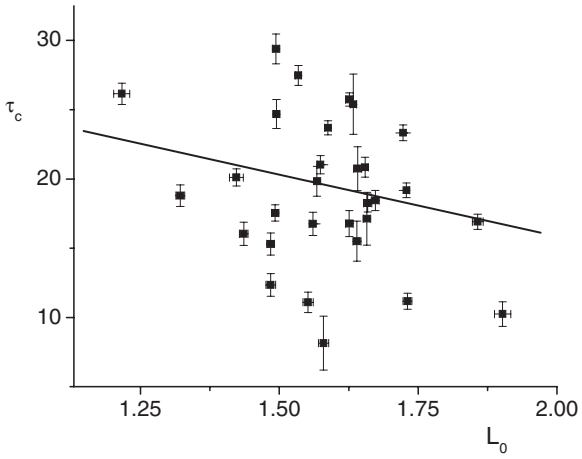

Figure 8. Same as in figure 5 except that here cells grow in minimal medium (M9-glucose).

particular, closure is slow for small t' and fast for t' close to unity. While during the first quarter of the T-period the waist width will decrease by only 3% (hardly visible), in the last quarter it decreases by 66%. As a result, the apparent T-period is much shorter than its full extent. Moreover, for most of the septation time the cell is only slightly partitioned, allowing free exchange of cytoplasmic constituents and unconstrained chromosome segregation. On the other hand, the elongation rate of the septal sector is constant during this period.

The assumptions that lead to equation (1) are confirmed by the good agreement between its predictions and the data. Moreover, the main assumption, namely that the area of the new caps grows at a constant rate, is directly verified in figure 1(*b*). It is worthwhile to stress that the accuracy with which this assumption holds is directly related to the error in the corresponding value of τ_c. On the other hand, the constancy of the septal area growth rate implies that there are a fixed number of peptidoglycan-forming complexes associated with the divisome and that these work at a steady specific activity during the T-period. The fact that there are a low number of FtsI molecules in the cell [6] is consistent with a permanent set of divisome subassemblies. The small number of these subassemblies may ensure that they will not collide with each other during Z-ring contraction until close to the end of division. As far as we know, this has never been experimentally verified.

For both fast and slow-growing cells, we found that, to a good approximation, τ_c and τ_g are linearly related while $\tau_g - \tau_c$ is independent of τ_g. Moreover, for fast-growing cells, τ_c is inversely correlated with L_0. The $\tau_c(L_0)$ correlation appears to be significantly weaker for slow-growing cells. This may be due to the larger fluctuations in the growth rates, a_1 and a_h, for slow-growing cells. It is interesting to note that although these fluctuations do not affect the variabilities of either τ_c or L_0 (these are similar for slow and fast-growing cells, see tables 1 and 2), they affect the accuracy of the relation between the two. This suggests that the relation $\tau_c(L_0)$ also depends on either a_1 or a_h or maybe on both. Both $\tau_c(\tau_g)$ and $\tau_c(L_0)$ relations may be viewed as compensation mechanisms. Long living cells will postpone initiating division for later times. Moreover, cells that are relatively long at birth will start to divide earlier. It seems that these two mechanisms act together in order to maintain a steady distribution of lengths, $P(L)$.

Since the T-period is approximately independent of τ_g (figures 4(*b*) and 7(*b*)), one expects that the timing of division is the main source of variability in the doubling time. This is likely to be related to the complexity of the self-assembly of the divisome. This process involves at least 13 proteins that need to be gathered in a specific order [1, 7]. The variability of each individual step of the divisome assembling sequence will build upon that of the previous steps in a cumulative manner. This mechanism of additive variability in a multi-step process may explain the observed large CV of τ_c.

The fact that constriction of the envelope starts at a particular time, τ_c, necessarily implies that a break point has to occur at this moment in the elongation dynamics of the cell. This break point was indeed observed in all the cells that were analyzed (figure 3(*c*)). In the elongation dynamics that is averaged over this population, the break point is smeared out (figure 3(*b*) and figure S2 in Supporting Data). This is the approach that was used in most studies of synchronous populations, e.g. [4, 11]. Only when using cell length distributions was it possible to identify the presence of a break point [5]. We emphasize that the presence of the break point at τ_c does not depend on whether the growth of L is approximated by a linear or exponential function of time before and after τ_c. At present, our measurements do not allow us to distinguish between linear versus exponential

growth dynamics. In order to be able to discern between the two possible behaviors, one will need to further improve the precision of the length measurements.

The comparison between fast and slow growth conditions, LB versus M9-glucose, shows that the observed phenomena, e.g. the break point in $L(t)$, the septum dynamics law of equation (1) and the correlations between τ_c, τ_g and L_0, are not specific to a particular growth rate. On one hand, LB as a culture medium is not as well defined as M9-glucose. It contains yeast extract which may be slightly different from one batch to another. Moreover, in fast-growing cells the overlap of DNA replication forks is large leading to a more complex cell division process. On the other hand, cells grown in M9-glucose are smaller in size. On average, these are about 1.5 times shorter and 1.3 times thinner than those grown in LB. Consequently, such cells represent a more difficult challenge for our contour finding algorithm leading to larger relative errors in both L and R. One may therefore expect that the study of fast-growing cells should be advantageous for reliably establishing the existence of the break point. Such expectation is further supported by the fact that the rate of septal elongation, a_h, decreases as the average generation time increases (see tables 1 and 2), resulting in a corresponding decrease in the change of slope of $L(t)$ at τ_c. However, due to the larger τ_c and $\tau_g - \tau_c$, the experimental errors of a_1 and a_2 are also smaller for slow-growing cells. In fact, the relative error for the change in the growth rate at τ_c is about equal for slow and fast-growing cells in our experiment. In other words, determining the presence of the breakpoint in $L(t)$ is equally difficult at both growth rates.

Similar single-cell morphogenesis studies were performed for the fission yeast *Schizosaccharomyces pombe* (reviewed in [15]). It was shown that cell growth is linear and takes place in two regimes separated by a break point in the rate of growth. It was referred to as a rate change point (RCP). A third regime associated with mitosis was also found during which the cell length is almost constant. The RCP was shown to be due to the start of growth at the new pole (NETO, which stands for 'new pole take off'). It was shown that both $L_g - L_0$ and τ_g are inversely proportional to L_0. Moreover, the pre-RCP time is inversely proportional to L_0, while the post-RCP extent of the second regime is independent of L_0. In other words, despite the fact that the physiology of *S. pombe* is quite different from that of *E. coli,* the two display similarities in the growth dynamics and size control phenomenology. Such similarities may prove useful in the search for the signal that initiates cell division in *E. coli*.

5. Conclusion and outlook

To conclude, in this work we demonstrate that precise monitoring of the single-cell global features provides new insights into the organization of the cell cycle. In particular, we have accurately timed the initiation and completion of septation and established the bimodal/trimodal elongation dynamics. To understand the processes underlying these phenomena at the molecular level, we should extend our approach to tracking the dynamics of the divisome protein constituents in individual cells. This work is underway.

Acknowledgments

We thank I Golding for suggesting the idea of data collapse, R Granek, K C Huang, Y Meir, E Moses, N Wingreen and A Zaritsky for useful discussions and J Rouviere-Yaniv for the bacterial strain.

Glossary

Z-ring. A ring structure consisting of FtsZ, a tubulin-like protein, that forms at the center of the bacterial cell sometime before the start of cell septation.

Divisome. The complex of the Z-ring and a group of proteins that together control bacterial cell division.

T-period. The time between the start of envelope septation until the end of bacterial cell division.

References

[1] Aarsman M E, Piette A, Fraipont C, Vinkenvleugel T M, Nguyen-Disteche M and den Blaauwen T 2005 Maturation of the *Escherichia coli* divisome occurs in two steps *Mol. Microbiol.* **55** 1631–45

[2] den Blaauwen T, Buddelmeijer N, Aarsman M E G, Hameete C M and Nanninga N 1999 Timing of FtsZ assembly in *Escherichia coli J. Bacteriol.* **181** 5167–75

[3] den Blaauwen T, Aarsman M E G, Vischer N O E and Nanninga N 2003 Penicillin-binding protein PBP2 of *Escherichia coli* localizes preferentially in the lateral wall and at mid-cell in comparison with the old cell pole *Mol. Microbiol.* **47** 539–47

[4] Cooper S 1988 Leucine uptake and protein synthesis are exponential during the division cycle of *Escherichia coli* B/r *J. Bacteriol.* **170** 436–8

[5] Cullum J and Vicente M 1978 Cell growth and length distribution in *Escherichia coli J. Bacteriol.* **134** 330–7

[6] Dougherty T J, Kenedy K, Kessler R and Pucci M 1996 Direct quantitation of the number of individual penicillin-binding proteins per cell in *Escherichia coli J. Bacteriol.* **178** 6110–5

[7] Goehring N W, Gonzalez M D and Beckwith J 2006 Premature targeting of cell division proteins to midcell reveals hierarchies of protein interactions involved in divisome assembly *Mol. Microbiol.* **61** 33–45

[8] Helmstetter C E 1996 Timing the synthetic activities in the cell cycle *Escherichia coli and Salmonella: Cellular and Molecular Biology* 2nd edn, ed F C Neidhardt, R Curtiss III, J L Ingraham, E C C Lin, K B Low, B Magasanik, W S Reznikoff, M Riley, M Schaechter and H E Umbarger (Washington, DC: ASM Press) pp 1627–39

[9] Hoffman H and Frank M E 1965 Time-lapse photomicrography of cell growth and division in *Escherichia coli J. Bacteriol.* **89** 212–6

[10] Itan E, Carmon G, Rabinovitch A, Fishov I and Feingold M 2008 The shape of non-septated *E. coli* is asymmetric *Phys. Rev.* E **77** 061902

[11] Kubitschek H E 1986 Increase in cell mass during the division cycle of *Escherichia coli* B/rA *J. Bacteriol.* **168** 613–8

[12] Nanninga N 1998 Morphogenesis of *Escherichia coli* *Microbiol. Mol. Biol. Rev.* **62** 110–29

[13] Reshes G, Vanounou S, Fishov I and Feingold M 2008 Cell shape dynamics in *E. coli Biophys. J.* **94** 251–64

[14] Schaechter M, Williamson J P, Hood J R and Koch A L 1962 Growth, cell and nuclear divisions in some bacteria *J. Gen. Microbiol.* **29** 421–34
[15] Sveiczer A, Novak B and Mitchison J 1996 The size control of fission yeast revisited *J. Cell Sci.* **109** 2947–57
[16] Trueba F J, Neijssel O M and Woldringh C L 1982 Generality of the growth kinetics of the average individual cell in different bacterial populations *J. Bacteriol.* **150** 1048–55
[17] Vollmer W and Holtje J-V 2001 Morphogenesis of *Escherichia coli Curr. Opin. Microbiol.* **4** 625–33
[18] Wery M, Woldringh C L and Rouviere-Yaniv J 2001 HU-GFP and DAPI co-localize on the *Escherichia coli* nucleoid *Biochimie* **83** 193–200